Hindawi
Geofluids
Volume 2020, Article ID 8836287, 14 pages
https://doi.org/10.1155/2020/8836287

Research Article

A Simplified Capillary Bundle Model for CO_2-Alternating-Water Injection Using an Equivalent Resistance Method

Wendong Wang,[1,2] **Fankun Meng**,[3] **Yuliang Su**,[1,2] **Lei Hou**,[4] **Xueyu Geng**,[4] **Yongmao Hao**,[1,2] **and Lei Li**[1,2]

[1]*Key Laboratory of Unconventional Oil & Gas Development, China University of Petroleum (East China), Ministry of Education, Qingdao 266580, China*
[2]*School of Petroleum Engineering, China University of Petroleum (East China), Qingdao 266580, China*
[3]*School of Petroleum Engineering, Yangtze University, Wuhan 430100, China*
[4]*School of Engineering, The University of Warwick, Coventry CV4 7AL, UK*

Correspondence should be addressed to Fankun Meng; mengfk09021021@163.com

Received 26 June 2020; Revised 26 September 2020; Accepted 29 October 2020; Published 29 November 2020

Academic Editor: Micòl Mastrocicco

CO_2-alternating-water injection is an effective way of enhancing recovery for low-permeability oil reservoirs. The injection process is one of the essential issues that are facing severe challenges because of the low permeability and poor pore space connectivity. Previous researchers mentioned that water injection ability could be decreased by around 20% after the CO_2-flooding; hence, it is necessary to quantify the water injectivity variation during an alternated injection process. In this paper, a CO_2 convection-diffusion model is established based on the seepage law of CO_2 and dissipation effect. The relationship between the width of miscible flooding and injection time is defined. Besides, an equivalent resistance method is introduced for developing a capillary bundle model for featuring an unequal diameter for CO_2 water vapor alternate flooding. CO_2-oil and CO_2-water interactions are analyzed using the new model. The effects of oil viscosity, pore throat ratio, CO_2 slug size, and equivalent permeability of the capillary bundle on water injection are analyzed. The result indicates that water injection ability increases with the rise of CO_2 slug size and equivalent permeability of the capillary bundle and decreases with the increase of viscosity and pore throat ratio.

1. Introduction

The CO_2-alternating-water injection method, used in the low-permeability reservoirs, has the advantages of both CO_2 flooding and water flooding. It represents a promising method for improving the recovery of oil in the future. In 1957, Mobil Company has performed a pilot CO_2-alternating-water injection test in North Pembina of Alberta, and then, several tests were conducted in Canada and the United States. In the United States, many tests have been performed because of the sufficient CO_2 sources [1, 2], whereas in China, the first pilot field application was started by CNOOC in Qikou oilfield. The test showed that during the middle-late stage of the nonhomogeneous reservoir, the CO_2-alternating-water injection could not only block the advantage flow channel but also contribute to the optimization of water injection [2]. Although its significant benefits, this method still has several problems. One serious problem is the decreasing of injection ability after CO_2-alternating-water has been injected into the formation [3, 4]. Therefore, it is significanlty important to study the variation of injection ability with capillary bundle model during CO_2-alternating-water flooding process.

The CO_2-alternating-water injection in the low-permeability reservoirs is a multiphase flow process. Early researchers have studied the seepage and flooding mechanism of multiphase fluid in the porous medium. Dong et al. presented the results of immiscible WAG injection in a water-wet micromodel and found that in a gas/oil/water system, stable oil layers were formed between the gas and water phases [5]. Due to gas bubbles were always surrounded by oil layers, direct

gas/water displacements were not observed. Meanwhile, he found that the oil recovery declined greatly with WAG cycles. Wang and Dong developed an interacting triangular tube bundle model based on capillaries of equilateral triangle cross sections [6]. The relationship between the residual oil saturation and the complete capillary number (CA) was investigated, and the effects of the tube size, tube size distribution, and viscosity ratio on the magnitude of entrapment were also studied using this tube bundle model. Jovanović et al. presented both the stagnant film model and the moving film model to study the energy loss problem when the fluid flows in the capillary [7]. They considered the interfacial pressure drop and the frictional pressure drop with the tube wall, and the influence of the static and fluid boundary layer on the fluid seepage. As microscopic flow mechanics gradually became the focus of investigation, some researchers began to pay attention to the complex seepage mechanism of pore space in porous media. Some of those researchers have been focusing on the alternate injection of water and gas by pore structure by establishing a pore network model as a simulation platform. Piri developed a quasi-static pore network model by fully considering the seepage characteristics of oil, gas, and water three-phase flow in the pore throat [8]. The variation of saturation and relative permeability of each phase in the process of water seepage are compared with the existing experiment, and the data is well fitted. Yang et al. simulated the WAG displacement process in different wettable porous media from a microscopic point of view and analyzed the oil, gas, and water saturation and distribution during WAG displacement [9]. The changed law of position and displacement characteristics explains the microscopic mechanism of three-phase seepage in porous media. Helland pointed out that a bundle-of-triangular-tube model can reproduce the main characteristics of mixed-wet capillary pressure curves with hysteretic scanning loops [10].

The displacement core test could be used to study the effect on the injection of CO_2-alternating-water process. Jinan et al. designed an experimental unit for long core displacement by considering the necessity of similarities upon core length, the complex mechanism, and periodic physical-chemical reaction during multicontact miscible phases [11]. Zhao et al. analyzed the affecting factors of CO_2 flooding, which include permeability, the relative density of crude oil, layer heterogeneity, interlayer heterogeneity, and layer fluid channeling by establishing the component numerical simulation model with Eclipse software [12, 13]. They concluded that it is appropriate to carry out CO_2 flooding for homogeneous and lightweight reservoirs in low-permeability oil fields. Zahoor et al. mentioned that proper water-alternating-gas process design and implementation requires better knowledge of wettability and wettability variations in particular [14]. Wettability, in addition to influencing flow parameters, strongly affects other design parameters such as the volumes of water and gas required for injection, well spacing, etc. Some other researchers also used experimental methods to study the increasing difficulty in injection. Prieditis et al. and Kamath et al. conducted displacement tests on carbonate and limestone cores and analyzed the factors that cause a decrease of injectivity [15, 16]. Prieditis et al. also performed a field test based on laboratory work and used a simple model to predict the injectivity, but good results were not achieved [15]. Roper et al. used a compositional model to simulate and interpret an injectivity test conducted in the Mabee Field in the San Andres Formation, Martin County, Texas [17, 18]. They mentioned that the validation of compositional simulation as a means for interpreting field tests and developing improved predictions of reservoir injectivity performance and geostatistical techniques could be used successfully to characterize high heterogeneity in carbonate reservoirs for injectivity calculations. Yang et al. used core samples collected from tight formations to conduct a series of water-alternating-CO_2 flooding experiments with different water-alternating-CO_2 ratios and slug sizes [19]. They found that fluid injectivity is strongly dependent on slug size, water-alternating-CO_2 ratio, and cycle time.

Besides the experimental work, early researchers have done some theoretical modeling work. Li et al. derived the injectivity equation for water-alternating-gas injection based on similarity theory [20]. Zhou et al. analyzed the effects of injection pressure, injection speed, slug size, and gas-water slug ratio on oil displacement efficiency [21]. Yan et al. used a numerical simulation method to study the best injection parameters for CO_2 gas water alternative drive [22]. Hu substituted the permeability of the capillary model into low-permeability equation and used superposition method to get total flow rate and threshold pressure gradient of the rock [23]. This model gives a theoretical description of low-permeability seepage characteristics. Several researchers have studied the injection capacity of different reservoirs and found that the injection volume, injection velocity, formation temperature, formation pressure segment size, and proportion have an impact on the final oil displacement efficiency and recovery factor [24–29]. Pizarro and Lake considered the influence of heterogeneity and autocorrelation of reservoir permeability distribution on the injectivity [30]. This model gives insight into why injectivity calculated from a core permeability average is frequently different from the injectivity manifested by the well in question. Yang et al. performed numerical simulations to history-match the experimental measurements and conduct sensitivity analysis on operational parameters and achieved good matching [19].

Overall, researchers have done relatively thorough research on the decreasing injectivity happens in low-permeability reservoir during CO_2 injection. However, due to the complexity of flow behavior of water-oil-gas, just a few researchers have explained the abnormal variance of injectivity during water-alternating-CO_2 injection. In this paper, a new seepage diffusion equation is established by considering the CO_2 diffusion and seepage in the reservoir. It could effectively reflect the variance of CO_2 injectivity in water-alternating-CO_2 injection process. The distribution of oil, CO_2, and water in the capillary model with different diameters has been analyzed, and the influence of geology and fluid properties on injectivity has been provided.

2. CO_2 Flooding Dynamics considering Mass Transfer

2.1. Mathematical Modeling. Assuming that the CO_2 flooding process in the capillary model is a piston, the molecular

diffusion, convective diffusion, and viscosity difference diffusion due to the difference of viscosity between CO_2 and crude oil will occur at the interface between CO_2 and crude oil. From a thermodynamic point of view, diffusion coefficients are functions of pressure, temperature, and composition, and driven by chemical potential difference; however, the proposed model is complex and hard to use [31]. Therefore, in this paper, the classical Fick's law is utilized. According to the classical Fick's law, molecular diffusion is mainly caused by the change of CO_2 concentration in crude oil, and the diffusion coefficients are assumed to be constant. Convective diffusion is mainly affected by the complexity of the internal channels of the pores. The diffusion under the viscosity gradient is related to the difference of viscosity between CO_2 and crude oil, and it is also affected by molecular diffusion and convection-diffusion [32]. The diffusion equation is derived from mass transfer equations by considering the balance of matter into and out of the capillary unit. To derive the diffusion equation of CO_2 in the capillary, here, a $\pi R^2 dx$ flowing unit of the capillary tube is studied (Figure 1).

According to the principle of material balance, the influent mass = effluent mass + amount of substance accumulated in the unit, which is as follows:

$$\frac{\partial C}{\partial t} = -\frac{\partial v_D}{\partial x} - \omega \frac{\partial C}{\partial x}. \tag{1}$$

According to the diffusion law,

$$v_D = -D\frac{\partial D}{\partial x}. \tag{2}$$

Substituting Equation (2) into Equation (1), the material diffusion equation of the flow unit in the capillary is obtained.

$$\frac{\partial C}{\partial t} + \omega \frac{\partial C}{\partial x} = \frac{\partial}{\partial x}\left(D\frac{\partial C}{\partial x}\right), \tag{3}$$

where C is a unit concentration of CO_2 after a mixed phase of crude oil and CO_2, %; D is a comprehensive diffusion coefficient, cm^2/s; ω is the flow velocity of the fluid in the capillary, cm/s. Here, the comprehensive diffusion coefficient D can be understood as a composite coefficient which not only considers the molecular diffusion and convection-diffusion of the single-phase fluid in the capillary but also considers the viscosity difference between the displacement and the displaced solution.

For the method of determining the diffusion coefficient, based on the Stokes-Einstein relation, Kooijman developed a correlation and used UNIFAC parameters to correct for particle roundness and size. Hayduk and Minhas developed a set of correlations, specific to certain types of mixtures. Sigmund developed a correlation for high-pressure gas and liquid binary mixtures with the expression that related the reduced density-diffusion coefficient product to a third-degree polynomial function of reduced density. For nonideal binary mixtures, Riazi and Whitson developed a correlation to predict gas and liquid diffusion coefficient. Currently, the most widely used correlation to calculate diffusion coefficient is presented by Wilke and Chang and is the function of viscosity, which is used in this paper [33].

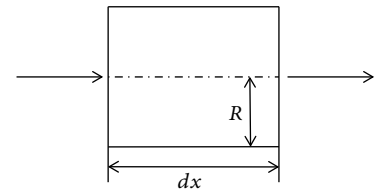

Figure 1: Flow unit of the capillary tube.

The results of a displacement experiment in which a liquid is miscible with another liquid in the presence of differential pressure indicate that the best approximation of the overall diffusion coefficient is as follows:

$$\begin{aligned} D &= D_E\left(1 + K_\mu \nabla \mu_m\right), \\ D_E &= D_m + D_\mu, \\ D_\mu &= K_\omega \omega, \end{aligned} \tag{4}$$

where D_m is the molecular diffusion coefficient, cm^2/s; D_u is the convection-diffusion coefficient of single-phase fluid, cm^2/s; μ_m is the viscosity of two liquid mixtures, mPa·s; K_ω and K_μ are the experimental coefficients which consider the experimental coefficients of single-phase fluid convection and different viscosity diffusion, with the unit of cm and cm/(MPa·s).

From Equation (4),

$$D = D_m + D_u + (D_m + D_u)K_\mu \nabla \mu_{m.} \tag{5}$$

Meanwhile,

$$D_\mu = (D_m + D_u)K_\mu \nabla \mu_m. \tag{6}$$

D_μ is the diffusion coefficient of viscosity difference between displacement fluid and displaced fluid. Equation (6) shows that the comprehensive diffusion coefficient is the sum of the molecular diffusion coefficient, the convection-diffusion coefficient, and the diffusion coefficient of the viscosity difference between the displacement fluid and the displaced fluid, which is a mixing coefficient.

2.2. Solution Strategy. In miscible region, we assume that there is only a single phase, which is the mixture of oil and gas phase. We introduced a new variable, $\tau = t, \xi = x - u/\phi$, into Equation (3). Then, Equation (3) become the standard diffusion equation.

$$\frac{\partial C}{\partial \tau} = \frac{\partial}{\partial \xi}\left(D\frac{\partial C}{\partial \xi}\right), \tag{7}$$

where ξ is called the self-modulation variable which changes with time and space.

The boundary conditions are as follows:

$$C(-\lambda, t) = 1, \tag{8}$$

$$C(\lambda, t) = 0, \tag{9}$$

$$C(0, t) = 0.5, \tag{10}$$

where $\pm\lambda$ is the miscible half-width, cm.

Also, it is assumed that there is no CO_2 inflow or outflow at the boundary of the miscible zone.

$$\left.\frac{\partial C}{\partial \xi}\right|_{\xi=\pm\lambda} = 0. \tag{11}$$

The viscosity of the miscible zone μ_m is also given in Figure 2 and is considered to be linear, so the viscosity of the miscible zone is as follows:

$$\nabla\mu_m = \frac{\mu_2 - \mu_1}{2\lambda}. \tag{12}$$

Assuming $\beta = K_\mu(\mu_2 - \mu_1/2)$, then $K_\mu\nabla\mu_m = \beta/\lambda$. Equation (7) becomes the following:

$$\frac{\partial C}{\partial \tau} = \frac{\partial}{\partial \xi}\left[D_E\left(1 + \frac{\beta}{\lambda}\right)\frac{\partial C}{\partial \xi}\right]. \tag{13}$$

After solving Equation (13), the differential form solution can be obtained as follows:

$$\frac{d\lambda}{d\tau} = 4D_E\frac{1}{\lambda}\left(1 + \frac{\beta}{\lambda}\right). \tag{14}$$

Thus, the corresponding "integral form solution" is given as follows:

$$\frac{\lambda^2}{2} - \beta\lambda + \beta^2 \ln\left(\frac{\lambda + \beta}{\beta}\right) = 4D_E\tau. \tag{15}$$

If the full length of the mixed-phase zone is $\Lambda = 2\lambda$, Equation (15) can be transformed as follows:

$$\frac{\Lambda^2}{4} - \beta\Lambda + 2\beta^2 \ln\left(\frac{\Lambda + 2\beta}{2\beta}\right) = 8D_E\tau. \tag{16}$$

Equations (15) and (16) can be used to calculate the half-width λ or width Λ of the miscible region at any given time t, and $\lambda = \lambda(t)$ and $\Lambda = \Lambda(t)$ can be obtained by the iterative method that can be used to solve.

3. Unequal Diameter Capillary Beam Model for CO_2-Alternating-Gas Flooding

3.1. Physical Model. It is assumed that the capillary beam model consists of n capillaries with different capillary radii. Since in real oil reservoir, for any one flowing path, there are pores and throats; therefore, to reflect this pattern, for each capillary, the radius is not equal everywhere along the axis, and there is a throat. For the ith capillary, the pore throat structure is as follows in Figure 3.

The capillary length is L, the throat position is L_c from the injection end of the capillary section, throat length is L_t, the capillary radius is R_p, and the radius at the throat is as follows:

$$R(x) = \left(\frac{R_p + R_t}{2}\right) + \left(\frac{R_p - R_t}{2}\right)\cos\left(\frac{2\pi x}{L_t}\right), \tag{17}$$

where R_t is the throat radius, μm; $R(x)$ is the radius of the junction of the pore and the throat, μm; x is between $0 \sim L_t$, cm; the total volume of the throat is as follows:

$$V = \pi\int_0^{L_t} R^2(x)dx. \tag{18}$$

According to the definition of alternate driving of water and gas, the injection process can be divided into two stages, namely, CO_2 injection and water injection. Because the throat is arbitrarily distributed for the same capillary, the throat position is various for different capillaries, and the fluid distribution in the capillary is complicated because of the difference in CO_2 injection time.

In the process of CO_2 injection, six distribution patterns exist in the crude oil, mixed-phase zone, and CO_2 in the capillary tube, and in the process of water flooding process, there are three fluid distribution patterns. Schematics and descriptions for those fluid distribution patterns are shown in Table 1.

3.2. CO_2 Flooding Seepage Mode and Mathematical Description. To facilitate the solution and analysis of the mathematical model, CO_2/water is injected by constant pressure. The injection pressure of each capillary is equal, and the pressure difference between the injection end and the production end is ΔP. Introducing the seepage resistance coefficient to describe the magnitude of the seepage resistance and using the equivalent resistance model to solve the capillary beam injection flow rate are as follows [34]:

3.2.1. Fluid Distribution Pattern I. For the ith capillary, at the beginning of time j ($j = 1, 2, 3, \cdots, N_{tg}$), when $x_{gi}^{j-1} + x_{\lambda i}^{j-1} < L_c$, the seepage resistance in the CO_2 zone is as follows:

$$W_{gi}^{j} = \frac{8\mu_g x_{gi}^{j-1}}{\pi R_{pi}^4}, \tag{19}$$

where $x_{gi}^{j-1} = 0$ is the length of CO_2 region at the $j-1$ moment for the ith capillary, cm; for the beginning, $x_{gi}^{0} = 0$. μ_g is the CO_2 viscosity, mPa·s; R_{pi} is the capillary radius, μm.

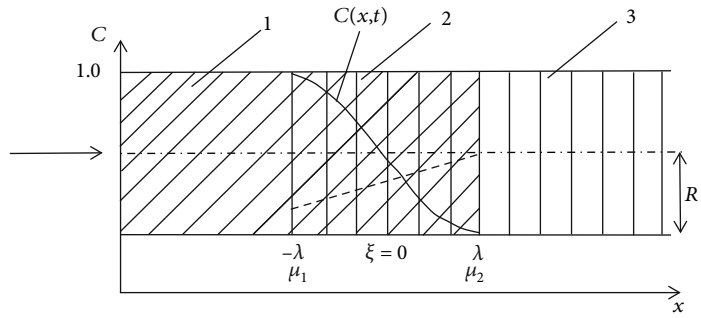

Figure 2: Schematic of CO_2 flooding (1: CO_2 region, 2: miscible region, and 3: oil region).

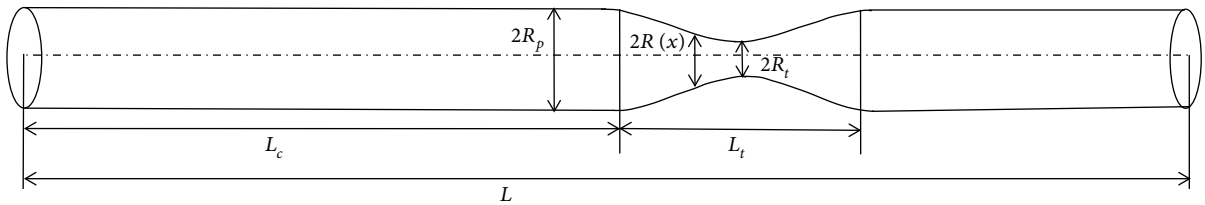

Figure 3: Structural schematic of pore and throat in the capillary tube.

The seepage resistance of the miscible zone is as follows:

$$W_{gi}^{j} = \frac{8\bar{\mu}_{og} x_{\lambda i}^{j-1}}{\pi R_{pi}^{4}}, \tag{20}$$

where $x_{\lambda i}^{j-1}$ is the miscible length at the moment of $j-1$, cm; for the beginning, $x_{gi}^{0} = 0$; $\bar{\mu}_{og}$ is the miscible fluid viscosity, mPa·s.

The seepage resistance in the crude oil zone is as follows:

$$W_{o,i}^{j} = \frac{8\mu_0\left(L - x_{gi}^{j-1} - x_{\lambda i}^{j-1} - L_{ti}\right)}{\pi R_{pi}^{4}} + \mu_0 \int_0^{L_{ti}} \frac{dx}{G(x)}, \tag{21}$$

where G is the conductivity of a fluid per unit length, μm^4.

$$G(x) = \frac{\pi}{128}\left(\sqrt{\frac{A_t}{\pi}} + R(x)\right)^4 = \frac{\pi}{8} R^4(x). \tag{22}$$

In the case of a constant pressure difference, the injection flow rate is as follows:

$$q_{gi}^{j} = \frac{\Delta P + P_{c,o-g}}{W_{eg}^{j}}, \tag{23}$$

where $W_{eq,i}^{j} = W_{g,i}^{j} + W_{\lambda,I}^{j} + W_{o,i}^{j}$, because there is no interfacial tension between CO_2 and crude oil, $P_{c,o-g} = 0$.

During the Δt time, it is assumed that the fluid seepage velocity in the capillary remains constant.

$$W_{i}^{j} = \frac{q_i^j}{\pi R_{pi}^{2}}. \tag{24}$$

The convection-diffusion coefficient between CO_2 and crude oil is as follows:

$$D_{Ei}^{j} = D_m + K_w W_{gi}^{j}. \tag{25}$$

According to the derivation in Section 2.2, the relationship for the length of miscible band at time j is obtained, and the relevant parameters are substituted. Using the Newton iteration method, the length of miscible band at the end of time j can be obtained. Since in Equation (1), C is defined as the unit concentration of CO_2 in the mixture phase; it also can be seen as the volume ratio of CO_2 in the unit bulk volume approximately, as shown in Figure 2. Therefore, assuming the volume of dissolved CO_2 in the miscible zone occupies 1/2 of its total volume, the amount of CO_2 dissolved in the mixed phase is as follows:

$$V_{misi}^{j} = \left(\frac{1}{2}\right)\pi R_{pi}^{2} x_{\lambda i}^{j}. \tag{26}$$

The length of the CO_2 zone formed at the beginning of the time $j+1$ is as follows:

$$x_{gi}^{j} = \frac{V_{gi}^{j}}{\pi R_{pi}^{2}} = x_{gi}^{j-1} + \frac{q_{g,i}^{j}\Delta t - V_{misi}^{j}}{\pi R_{pi}^{2}}. \tag{27}$$

Table 1: Schematics for fluid distribution pattern during CO_2 and water flooding.

Process	Number	Fluid distribution pattern	Description
CO_2 flooding	I	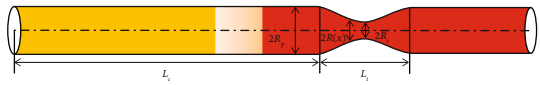	The front edge of the mixed-phase zone does not enter into the throat; the fluid in the throat is crude oil.
	II	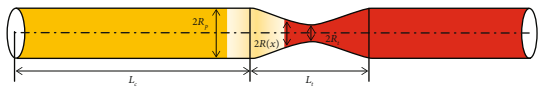	The front of the CO_2 flooding is not entering the throat, but the right end of the miscible belt has entered the throat and occupied a part of the throat.
	III	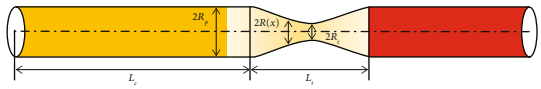	The front of the CO_2 flooding is not entering the throat, but the right end of the miscible belt has entered the throat and occupied a part of the throat.
	IV	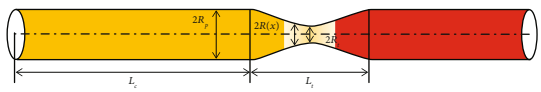	The leading edge of the CO_2 displacement has not entered the throat, the volume of the mixed phase is larger than the volume of the throat, and the right end has passed through the throat.
	V	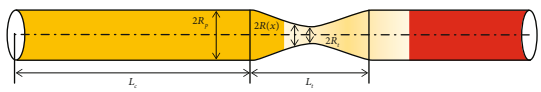	The leading edge of the CO_2 displacement enters into the throat, and the right end of the miscible zone passes through the throat.
	VI	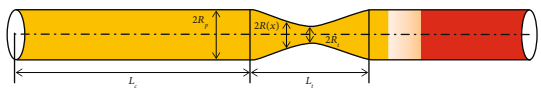	The leading edge of CO_2 displacement passes through the throat and the throat is filled with CO_2.
Water flooding	VII	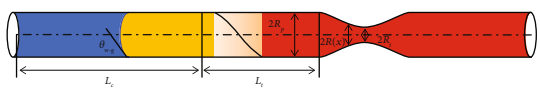	Water leading edge does not enter the throat.
	VIII	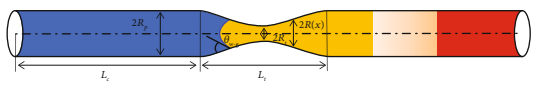	Water leading edge enters the throat.
	IX	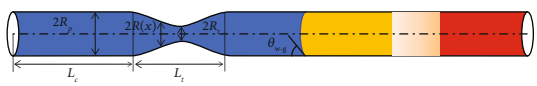	Water leading edge passes through the throat.

The total amount of CO_2 injected into the bundle of tubes is as follows:

$$Q_g^j = \sum_{i=1}^{n} q_{g,i}^j. \tag{28}$$

If the calculated sum of the CO_2 zone x_{gi}^j and the miscible zone $x_{\lambda i}^j$ is less than L_{ci}, iterative calculation of $j+1$ time can be performed according to the above steps.

3.2.2. Fluid Distribution Pattern II. At the beginning of j_n moment, when the sum of the obtained CO_2 zone and the miscible zone length is greater than L_{ci}, but the volume of the miscible belt is smaller than the volume of the throat, that is $x_{gi}^{j_n-1} + x_{\lambda i}^{j_n-1} \geq L_{ci}$, $x_{gi}^{j_n-1} \leq L_{ci}$, $2V_{misi}^{j_n-1} < V_{ti}$. At the end of the $j_n - 1$ moment, the length of the miscible belt in the throat $L_{\lambda i}^k$ $(k = 1, k = k + 1)$ is as follows:

$$\left(x_{gi}^{j_n-1} + x_{\lambda i}^{j_n-1} - L_{ci}\right) R_{pi}^2 = \int_0^{L_{\lambda i}^k} R^2(x)dx. \tag{29}$$

The Lobatto numerical integral formula can be used to solve $L_{\lambda i}^k$; $x_{\lambda i}^{j_n-1}$ is the equivalent length of the miscible band, cm; the actual width of the miscible band is $x_{\lambda i}^{j_n-1} = L_{ci} - x_{gi}^{j_n-1} + L_{\lambda i}^k$. Meanwhile, the actual length of the crude oil zone is $x_{oi}^{j_n-1} = L - L_{ci} - L_{\lambda i}^k$.

The seepage resistance of the miscible zone includes two parts, one is the seepage resistance in the capillary at the left end of the throat and the other is the percolation resistance in the throat. The expression is as follows:

$$W_{\lambda,i}^{j_n-1} = \frac{8\bar{\mu}_{og}\left(L_{ci} - x_{gi}^{j_n-1}\right)}{\pi R_{pi}^4} + \bar{\mu}_{og}\int_0^{L_{\lambda,i}^k} \frac{dx}{G(x)}. \tag{30}$$

The percolation resistance of crude oil and CO_2 in the capillary is as follows:

$$W_{o,i}^{j_n} = \mu_0 \int_{L_{\lambda,i}^k}^{L_{ti}} \frac{dx}{G(x)} + \frac{8\mu_0(L - L_{ci} - L_{ti})}{\pi R_{pi}^4}, \tag{31}$$

$$W_{g,i}^{j_n} = \frac{8\mu_o x_{gi}^{j_n-1}}{\pi R_{pi}^4}. \tag{32}$$

At the end of j_n moment, the injection amount of the ith capillary and the total injection amount of the capillary beam CO_2 can be calculated by Equations (23) and (28). At this time, the leading edge of CO_2 displacement is still outside the throat. Using Equations (27) and (26), the length of the CO_2 zone, $x_{gi}^{j_n}$, and the length of the equivalent miscible zone CO_2, $x_{\lambda i}^{j_n}$, at the end of j_n can be obtained (regardless of the length of the throat).

3.2.3. Fluid Distribution Pattern III. At the beginning of j_n moment, when the sum of the lengths of the CO_2 region and the miscible region is greater than L_{ci}, that is, ${x_{gi}}^{jn-1} + {x_{\lambda i}}^{jn-1} \geq L_{ci}$, ${2V_{mist}}^{jn-1} > V_n$, it indicates that at the beginning of j_n, the right end of the miscible band has begun to pass through the throat. The length of each zone and the seepage resistance are shown in Equations (30)–(32). The same iterative calculation procedure as in mode (2) is used to obtain the capillary tube injection flow rate.

The length of the miscible zone formed at the right end of the throat is $x_{r\lambda i}^m$ ($m = 1$, $m = m + 1$), and the expression is as follows:

$$x_{r\lambda i}^m = \left(x_{gi}^{j_d} + x_{\lambda i}^{j_d} - L_{ci}\right) - \frac{\left[\int_0^{L_{ti}} R^2(x)dx\right]}{R^2}. \tag{33}$$

The actual miscible band width is $x_{\lambda i}^{j_d} = L_{ci} - x_{gi}^{j_d} + L_{ti} + x_{r\lambda i}^m$. $x_{\lambda i}^{j_d}$ is the length of the equivalent miscible region at the end of j_d moment. The expression of seepage resistance in the miscible zone is as follows:

$$W_{\lambda,i}^{j_d+1} = \frac{8\bar{\mu}_{og}\left(L_{ci} - x_{gi}^{j_d} + x_{r\lambda i}^m\right)}{\pi R_{pi}^4} + \bar{\mu}_{og}\int_0^{L_t} \frac{dx}{G(x)}. \tag{34}$$

The seepage resistance of the CO_2 zone and the crude oil zone in the capillary is as follows:

$$W_{gi}^{j_d+1} = \frac{8\mu_g x_{gi}^{j_d}}{\pi R_{pi}^4}, \tag{35}$$

$$W_{o,i}^{j_d+1} = \frac{8\mu_o(L - L_c - L_t - x_{r\lambda i}^m)}{\pi R_{pi}^4}. \tag{36}$$

At this time, CO_2 flooding interface is still outside the throat. Using Equations (27) and (26), the length of the CO_2 zone at the end of $j_d + 1$ is $x_{gi}^{j_d+1}$, and the length of the equivalent miscible zone is $x_{\lambda,i}^{j_d+1}$. At this time, it is necessary to judge the relative size of $x_{gi}^{j_d+1}$ and L_{ci}. If $x_{gi}^{j_d+1} \leq L_{ci}$, the iterative calculation can be continued according to the steps in the distribution pattern II.

3.2.4. Fluid Distribution Pattern IV. Let CO_2 entering length is L_{gi}^a ($a = 1$, $a = a + 1$), and the expression is as follows:

$$\left(x_{gi}^{j_m} - L_{ci}\right)R_{pi}^2 = \int_0^{L_{gi}^a} R^2(x)dx, \tag{37}$$

where $x_{gi}^{j_m}$ is the equivalent length of the CO_2 zone, cm; actual length is $x_{gi}^{j_m} = L_{ci} + L_{gi}^a$.

It is assumed that after the CO_2 flooding leading edge enters the throat, CO_2 is no longer dissolved in the crude oil, and the equivalent length of the CO_2 zone remains constant. At the end of j_m, the seepage resistance in the CO_2 zone is as follows:

$$W_{gi}^{j_m+1} = \frac{8\mu_g L_{ci}}{\pi R_{pi}^4} + \mu_g \int_0^{L_{gi}^a} \frac{dx}{G(x)}. \tag{38}$$

Since the volume of the miscible zone is smaller than the throat volume, the actual length of the miscible zone in the throat at the end of j_m is $x_{\lambda i}^{j_m} = L_{\lambda I}^k - L_{gi}^a$ (k has been accumulated), where $L_{\lambda i}^k$ can be defined by the following:

$$R_{pi}^2 x_{\lambda i}^{j_m} = \int_{L_{gi}^a}^{L_{\lambda I}^k} R^2(x)dx, \tag{39}$$

where $x_{\lambda i}^{j_m}$ is the end of j_m, the equivalent length of the miscible band, cm.

Since CO_2 does not dissolve into the crude oil when the CO_2 flooding leading edge is in the throat, the equivalent length of the miscible zone remains constant until the CO_2 flooding leading edge passes through the throat. The seepage resistance of the miscible zone is as follows:

$$W_{\lambda,i}^{j_m+1} = \bar{\mu}_{og} \int_{L_{gi}^a}^{L_{\lambda i}^k} \frac{dx}{G(x)}. \tag{40}$$

The actual length of oil zone is $x_{oi}^{j_m} = L - L_{ci} - L_{ti} + (L_{ti} - L_{\lambda i}^k)$. The seepage resistance in the crude oil zone is as follows:

$$W_{o,i}^{j_m+1} = \frac{8\mu_o(L - L_{ci} - L_{ti})}{\pi R_{pi}^4} + \mu_o \int_{L_{\lambda i}^k}^{L_{ti}} \frac{dx}{G(x)}. \tag{41}$$

At the end of j_m, the length of the formed CO_2 zone is as follows:

$$x_{gi}^{j_m+1} = x_{gi}^{j_m} + \frac{q_{g,i}^{j_m+1}\Delta t}{\pi R_{pi}^2}. \tag{42}$$

The amount of CO_2 injected in the ith capillary and the total injection amount of the capillary bundle can be calculated by Equations (23) and (28).

3.2.5. Fluid Distribution Pattern V. At this time, the length of the miscible band formed in the capillary at the right end of the throat is $x^b_{r\lambda i}$ ($b = 1$, $b = b + 1$).

$$x^b_{r\lambda i} = x^{j_m}_{\lambda i} - \frac{\left[\int_{L^a_{gi}}^{L_{ti}} R^2(x)dx\right]}{R^2_{pi}}. \tag{43}$$

The actual width of the miscible band is $x^{j_m}_{\lambda i} = L_{ti} - L^a_{gi} + x^b_{r\lambda i}$. At the beginning of $j_m + 1$, the seepage resistance of the miscible zone is as follows:

$$W^{j_m+1}_{\lambda,i} = \frac{8\bar{\mu}_{og}x^b_{r\lambda i}}{\pi R^4_{pi}} + \bar{\mu}_{og}\int_{L^a_{gi}}^{L_{ti}} \frac{dx}{G(x)}. \tag{44}$$

The actual length of oil zone is $x^{j_m}_{oi} = L - L_{ci} - L_{ti} - x^b_{r\lambda i}$, and the seepage resistance in the crude oil zone is as follows:

$$W^{j_m+1}_{o,i} = \frac{8\mu_o\left(L - L_{ci} - L_{ti} - x^b_{r\lambda i}\right)}{\pi R^4_{pi}}. \tag{45}$$

The seepage resistance in the CO_2 zone is shown in Equation (38). The CO_2 injection amount in the ith capillary and the total injection amount in the capillary bundle can be obtained by Equations (23) and (28). The equivalent length of the miscible zone is constant, and the length of the formed CO_2 zone can be obtained by Equation (42).

3.2.6. Fluid Distribution Pattern VI. In the capillary, at the right end of the throat, the length of CO_2 region formed by x^c_{rgi} ($c = 1$, $c = c + 1$) is as follows:

$$\frac{q^{j_c}_{g,i}\Delta t - \int_{L^a_{gi}}^{L_{ti}} \pi R^2(x)dx}{\pi R^2_{pi}} = x^c_{rgi}. \tag{46}$$

At this moment, the CO_2 displacement front is outside the throat and CO_2 will continue to diffuse into the crude oil. At the beginning of $j_c + 1$, the actual length of the CO_2 zone is $x^{j_c}_{gi} = L_{ci} + L_{ti} + x^c_{rgi}$. The equivalent length of the miscible band is $x^{j_c}_{\lambda i}$, cm. Thereafter, the equivalent length of the miscible zone is equal to the actual length, and the actual length of the crude oil zone is $x^{j_c}_{oi} = L - x^{j_c}_{gi} - x^{j_c}_{\lambda i}$.

At the beginning of $j_c + 1$, the seepage resistance in the CO_2 zone is as follows:

$$W^{j_c+1}_{g,i} = \frac{8\mu_g\left(L_{ci} + x^c_{rgi}\right)}{\pi R^4_{pi}} + \mu_g\int_0^{L_{ti}} \frac{dx}{G(x)}. \tag{47}$$

The seepage resistances of the miscible zone and the crude oil zone are as follows:

$$W^{j_c+1}_{\lambda,i} = \frac{8\bar{\mu}_{og}x^{j_c}_{\lambda i}}{\pi R^4_{pi}}, \tag{48}$$

$$W^{j_c+1}_{o,i} = \frac{8\mu_o\left(L - x^{j_c}_{gi} - x^{j_c}_{\lambda i}\right)}{\pi R^4_{pi}}. \tag{49}$$

Knowing the magnitude of seepage resistance in each zone, the amount of CO_2 injection in the ith capillary and capillary bundle can be calculated by using Equations (23) and (28). According to Equations (47)–(49), combined with the formula of the mixed-phase band in Section 2, the length of CO_2 zone and the miscible zone can be obtained. Here, it should be noted that since the length of the miscible slug is constant when the leading edge of the CO_2 displacement is assumed to be in the throat, the calculation of the miscible zone is performed after deducting the period of the CO_2 displacement leading edge through the throat. In this way, according to the distribution pattern VI, the next iterative calculation is performed.

3.3. Water Flooding Seepage Mode and Mathematical Description. Suppose that the CO_2 injection time is T_g, the time step has N_{tg} ($N_{tg} = T_g/\Delta t$). At the beginning of $N_{tg} + 1$, the water is injected with a constant pressure difference, ΔP. Assuming that CO_2 is not dissolved in water, there is a gas-water interface. There is a capillary force, the CO_2-water interfacial tension is σ_{wg}, and the contact angle is θ_{w-g}. At the beginning of water injection, when the leading edge of CO_2 flooding is at the left end of the throat, during the subsequent water injection process, there may be six distribution patterns in the CO_2 flooding process, but on the other hand, due to water injection, the following three fluid distribution patterns appear.

3.3.1. Fluid Distribution Pattern VII. At this time, the seepage resistance of the water zone is as follows:

$$W^j_{w,i} = \frac{8\mu_w x^{j-1}_{wi}}{\pi R^4_{pi}}, \tag{50}$$

where x^{j-1}_{wi} is the length of the water zone in the capillary at the beginning of $N_{tg} + j$, cm, $x^0_{wi} = 0$.

The pressure difference between the ends of the capillary bundle is $\Delta P + P_{ci}$, which is kept constant, and the flow rate of injected water is as follows:

$$\begin{aligned} q^j_{w,i} &= \frac{\Delta P + P_{ci}}{W^{N_{tg}+j}_{eq,i}}, \\ P_{ci} &= \frac{2\sigma_{w-g}\cos\theta_{w-g}}{R_{pi}}, \end{aligned} \tag{51}$$

where $W^{N_{tg}+j}_{eq,i} = W^j_{wi} + W^{N_{tg}+j}_{g,i} + W^{N_{tg}+j}_{\lambda,i} + W^{N_{tg}+j}_{o,i}$, $W^{N_{tg}+j}_{g,i}$, $W^{N_{tg}+j}_{\lambda,i}$, $W^{N_{tg}+j}_{o,i}$ is the magnitude of seepage resistance in the CO_2 zone, the miscible zone, and the crude oil zone at the beginning of $N_{tg} + j$.

The total amount of water injected is as follows:

$$Q^{N_{tg}+j}_w = \sum_{i=1}^{n} q^{N_{tg}+j}_{w,i}. \tag{52}$$

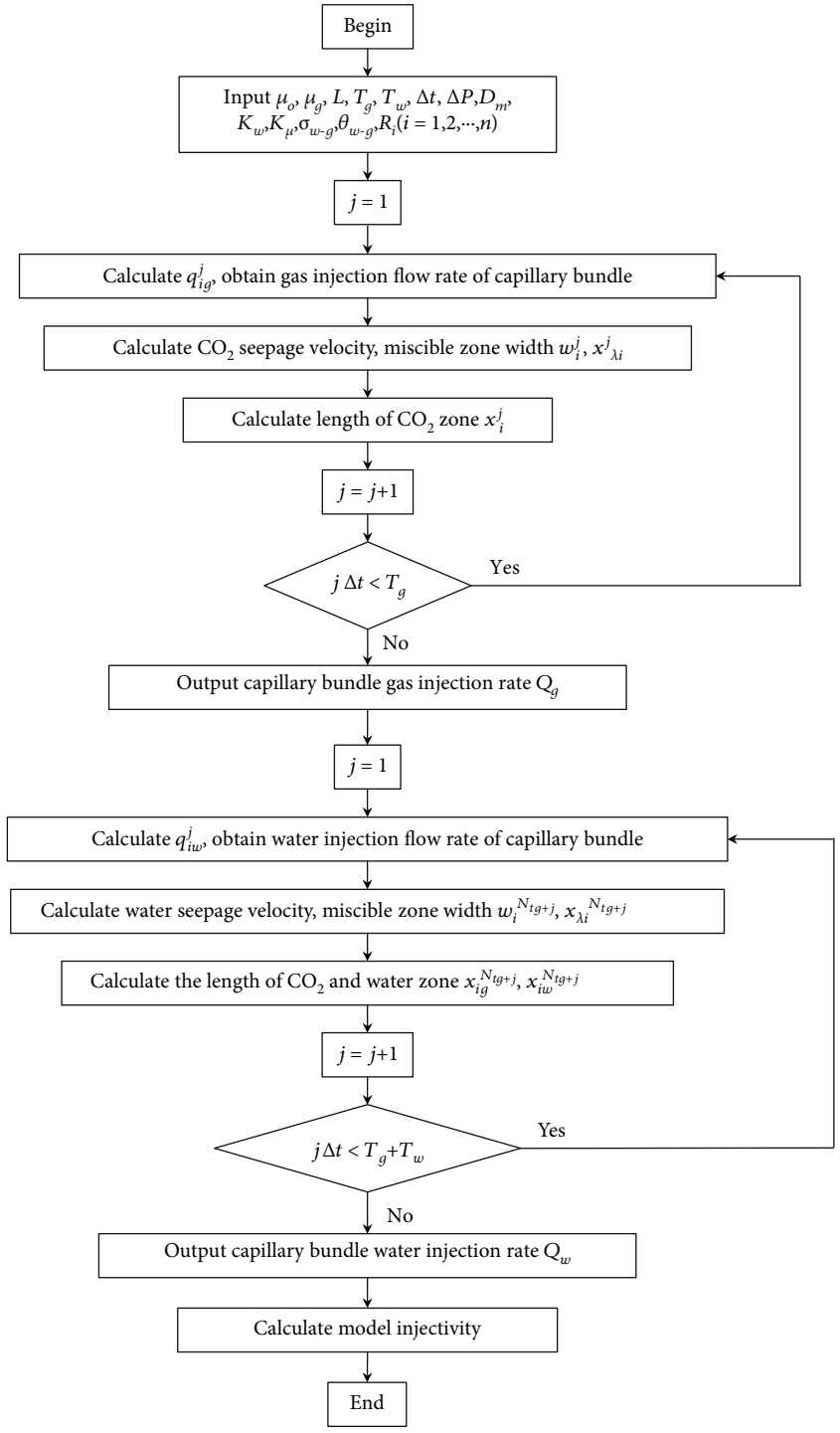

Figure 4: Flow diagram of solution.

During this process, the water seepage velocity is the same as CO_2.

$$W_{wi}^j = \frac{q_{w,i}^j}{\pi R_{pi}^2} = W_{gi}^{N_{tg}+j}. \tag{53}$$

According to the principle of material balance, due to the constant total injection volume, CO_2 will continue to diffuse into the crude oil during the water injection process, the length of the CO_2 zone and the crude oil zone will decrease, the width of the miscible zone will increase, and the calculation formula of the miscible zone will be for the distribution mode. For the first, second, third, and sixth fluid distribution pattern, the formula for calculating the length of the CO_2 zone should be corrected to the following:

$$x_{gi}^{N_{tg}+j} = x_{gi}^{N_{tg}+j-1} - \frac{\Delta V_{misi}^{j}}{\pi R_{pi}^2}, \tag{54}$$

where $\Delta V_{mist}^{j}$is the amount of increase in the amount of CO_2 dissolved in the miscible zone, cm^3; $x_{gi}^{N_{tg}+j}$ and $x_{gi}^{N_{tg}+j-1}$ are the equivalent lengths of the CO_2 zone at the time of $N_{tg}+j$ and $N_{tg}+j-1$, cm.

$$\Delta V_{misi}^{j} = V_{misi}^{N_{tg}+j} - V_{misi}^{N_{tg}+j-1} = \frac{1}{2}\pi R_{pi}^2\left(x_{\lambda i}^{N_{tg}+j} - x_{\lambda i}^{N_{tg}+j-1}\right), \tag{55}$$

where $x_{\lambda i}^{N_{tg}+j}$ and $x_{\lambda i}^{N_{tg}+j-1}$ are the equivalent lengths of the miscible band at the time of $N_{tg}+j$ and $N_{tg}+j-1$. Since the diffusion of CO_2 in water is not considered, the length of water zone in the capillary is as follows:

$$x_{wi}^{j} = x_{wi}^{j-1} + \frac{q_{wi}^{j}\Delta t}{\pi R_{pi}^2}. \tag{56}$$

3.3.2. Fluid Distribution Pattern VIII. Assuming at the beginning of $N_{tg}+j_w+1$ moment (which is also at the end of $N_{tg}+j_w$ moment), the length of water zone is calculated as $x_{wi}^{j_w} > L_{ci}$. It means that at the end of $N_{tg}+j_w$, the injected water has entered the throat. The length needs to be corrected, and the actual water zone length is $x_{wi}^{j_w-1}$.

$$x_{w,i}^{j_w} = L_{ci} + L_{wi}^{d}, \tag{57}$$

$$R_{pi}^2\left(x_{wi}^{j_w} - L_{ci}\right) = \int_0^{L_{wi}^{d}} R^2(x)dx, \tag{58}$$

where $x_{wi}^{j_w}$ is the equivalent length of the initial water zone at the time of $N_{tg}+j_w+1$, cm. L_{wi}^{d} $(d=1,\ d=d+1)$ is the extended length of the injected water in the throat.

In the throat, the radius of the water-CO_2 interface changes, so it will affect the capillary force. The capillary radius and capillary force at L_{wi}^{d} are as follows:

$$R_i\left(L_{wi}^{d}\right) = \left(\frac{R_P + R_t}{2}\right) + \left(\frac{R_p - R_t}{2}\right)\cos\left(\frac{2\pi L_{wi}^{d}}{L_t}\right), \tag{59}$$

$$P_{ci}^{d} = 2\sigma_{w-g}\cos\frac{\theta+\gamma}{R_i(x)}, \tag{60}$$

$$\gamma = \tan^{-1}\left(\frac{dR(x)}{dx}\right), \tag{61}$$

$$\tan\gamma = \frac{dR(x)}{dx} = \frac{R_i\left(L_{wi}^{d}\right) - R_i\left(L_{wi}^{d-1}\right)}{L_{wi}^{d} - L_{wi}^{d-1}}, \tag{62}$$

where $R_i(L_{wi}^{0}) = R_{pi}$, $L_{wi}^{0} = 0$; γ is the correction value of the contact angle.

At the beginning of $N_{tg}+j_w+1$, the actual CO_2 equivalent length is $x_{gi}^{N_{tg}+j_w}$, where the extension length at the right end of the throat is x_{rgi}^{e} $(e=1,\ e=e+1)$.

$$x_{rgi}^{e} = x_{gi}^{N_{tg}+j_w} - \frac{\int_{L_{wi}^{d}}^{L_{ti}} R(x)^2 dx}{R_{pi}^2}. \tag{63}$$

The seepage resistances in the water area and CO_2 area are given in Equations (64) and (65).

$$W_{w,i}^{N_{tg}+j_w+1} = \frac{8\mu_w L_{ci}}{\pi R_{pi}^4} + \mu_w\int_0^{L_{wi}^{d}}\frac{dx}{G(x)}, \tag{64}$$

$$W_{g,i}^{N_{tg}+j_w+1} = \frac{8\mu_g x_{rgi}^{e}}{\pi R_{pi}^4} + \mu_g\int_{L_{wi}^{d}}^{L_{ti}}\frac{dx}{G(x)}. \tag{65}$$

At this time, the length of the crude oil zone is $L - L_{ci} - L_{ti} - x_{rgi}^{e} - x_{\lambda i}^{N_{tg}+j_w}$, and the resistance of the crude oil zone can be obtained by substituting Equation (49), and the seepage resistance of the mixed phase can be obtained by using Equation (48). By substituting the formula for seepage resistance in each zone into Equations (51) and (52), the water injection amount of the ith capillary and capillary bundle can be obtained. According to Equations (51)-(55), the length of the water zone and the CO_2 zone can be obtained, and the method of obtaining the miscible zone is the same as in previous cases.

3.3.3. Fluid Distribution Pattern IX. At the beginning of $N_{tg}+j_g+1$, if the calculated L_{wi}^{d} is greater than L_{ti}, the water-CO_2 interface has passed through the throat, and the length formed at the right end of throat is x_{wri}^{e} $(e=1,\ e=e+1)$, $x_{wri}^{e} = x_{wi}^{j_g} - L_{ci} - [\int_0^{L_{ti}} R_i^2(x)dx]/R_{pi}^2$.

At the end of $N_{tg}+j_g$, the actual length of the water area is $x_{wi}^{j_g} = L_{ci} + L_{ti} + x_{wri}^{e}$. $x_{wi}^{j_g}$ is the equivalent length of water zone, the length of CO_2 zone is $x_{gi}^{N_{ig}+j_g}$, the length of miscible zone is $x_{\lambda i}^{N_{ig}+j_g}$, and the length of the crude oil zone is $L - L_{ci} - L_{ti} - x_{\lambda i}^{N_{tg}+j_g} - x_{gi}^{N_{tg}+j_g} - x_{wri}^{e}$. Water-$CO_2$ interfacial tension remains constant.

At the beginning of $N_{tg}+j_g+1$, the seepage resistance for each zone is as follows:

$$W_{w,i}^{N_{tg}+j_g+1} = \frac{8\mu_w(L_{ci}+x_{wri}^{e})}{\pi R_I^4} + \mu_w\int_0^{L_{ti}}\frac{dx}{G(x)}, \tag{66}$$

$$W_{g,i}^{N_{tg}+j_g+1} = \frac{8\mu_g x_{gi}^{N_{tg}+j_g}}{\pi R_i^4}, \tag{67}$$

$$W_{\lambda,i}^{N_{ig}+j_g+1} = \frac{8\bar{\mu}_{og} x_{\lambda i}^{N_{tg}+j_g}}{\pi R_i^4}, \tag{68}$$

$$W_{o,i}^{N_{tg}+j_g+1} = \frac{8\mu_o\left(L - x_{wi}^{j_g} - x_{gi}^{N_{tg}+j_g} - x_{\lambda i}^{N_{tg}+j_g}\right)}{\pi R_i^4}. \tag{69}$$

Table 2: Parameters for CO_2 water-alternating-gas model.

Parameters	Value	Parameters	Value
Capillary radius (μm)	5~15	Capillary length (cm)	30
Water/CO_2 interfacial tension (mN/m)	20	Water/CO_2 contact angle (degree)	60
Crude oil viscosity (mPa·s)	5	CO_2 viscosity (mPa·s)	0.05
Water viscosity (mPa·s)	2	K_w (cm)	0.001
K_μ(cm/(Pa•s))	0.001	CO_2 injection time (s)	5
D_m (cm^2/s)	1×10^{-5}	Time interval (s)	0.1
Injection time (s)	5	Pore throat ratio	3
Pressure difference at both ends of the capillary bundle (MPa)	1	Distance between throat and inlet end (cm)	2~3
Throat length (cm)	1	Number of capillaries	11

Substituting Equations (66)-(69) into Equations (51)-(55), the length of the water zone and the CO_2 zone can be obtained, and the parameters such as β and D_E are substituted into Equation (40) to obtain the width of the miscible zone.

4. Sensitivity Analysis

4.1. Model Solving Process and Basic Parameter Settings. According to the above descriptions, the solution process can be divided into two steps, CO_2 injection and water injection, and the flow chart of solution is shown in Figure 4.

During water-alternating-gas flooding process, the injection capacity is defined as the ratio of injected CO_2/water rate to the pressure difference across the capillary bundle:

$$I = \frac{Q_{w,g}}{\Delta P_{w,g}}, \tag{70}$$

where I is the injection capacity, cm^3/(MPa·s); $Q_{w,g}$ is the CO_2/water injection flow rate, cm^3/s; $\Delta P_{w,g}$ is the pressure difference across the capillary beam, MPa.

For the convenience of analysis, it is stipulated that during the injection of CO_2 and water injection, the pressure difference across the capillary bundle is equal. To quantitatively characterize the ability of the capillary tube to flow, the equivalent permeability is introduced, and the expression is as follows:

$$k = \frac{L}{8\sum_{i=1}^{n} R_{pi}^2 \left(\left(1/R_{pi}^4 \right) + \left(\int_0^{L_{ti}} \left(1/R_i^4(x) \right) dx \right) \right)}. \tag{71}$$

According to the variables used in the model derivation process, the pore throat size of the reservoir in low-permeability reservoirs and the characteristics of fluid properties of water-alternating-CO_2 injection are investigated [35], and the basic parameters of the model are set, as shown in Table 2.

4.2. Injection Capacity Analysis. To better reflect the change law of injectivity of CO_2, mixed-phase slug, and injection capacity, the throat is set closer to the injection end. Then, the influences of viscosity, pore throat ratio, CO_2 slug size, and equivalent permeability on the variance of CO_2-alternating-water capacity have been studied.

4.2.1. Crude Oil Viscosity. Assuming the crude oil viscosities are 5 mPa·s, 6 mPa·s, and 7 mPa·s, and simultaneously keep all other parameters constant, the changing law of injectivity with time is plotted in Figure 5.

As it can be seen from Figure 5, the crude oil viscosity increases, and the viscous resistance that the fluid flow needs to overcome increases, thus causing the injectivity to decrease as the crude oil viscosity increases. After the capillary beam is transferred to water, the high-viscosity crude oil is driven out. Then, the total seepage resistance of the fluid in the capillary bundle is reduced, causing the increase of injectivity. However, when the water-flooding front enters the throat, the low-viscosity CO_2 is replaced. Then, the seepage resistance is increased, causing a decrease of injectivity. As the fluid percolation velocity decreases with the increase of the crude oil viscosity, the time that the front of the water flooding enters the throat continuously is delayed with the increase of the crude oil viscosity. When the water-gas interface, that is, the front edge of the water drive passes through the throat, the throat is occupied by water, the displacement will tend to be stable, and the water injection capacity will continue to increase.

4.2.2. Pore Throat Ratio. Since the capillary radius has been set to characterize the pore size, the pore throat ratio is defined as the ratio of the capillary radius to the radius at the narrowest point of the throat. Set them to 2.5, 3, and 3.5, respectively, and the injection capacity changes with time are shown in Figure 6.

When the capillary radius is constant (the pore radius is constant), the throat radius decreases with the increase of the pore throat ratio. Because the throat size has a great influence on the seepage resistance, the CO_2 water-gas alternate injection capacity decreases with the increase of throat ratio. The throat is closer to the injection end, and after the water is injected, the injectivity is increased because the crude oil in the capillary bundle is replaced by the injected water. Similar to Figure 5, the front edge of the water drive enters the throat, and the injectivity is rapidly reduced; after the front edge passes through the throat, the injection capacity well increase slowly. Because the seepage resistance generated by the fluid

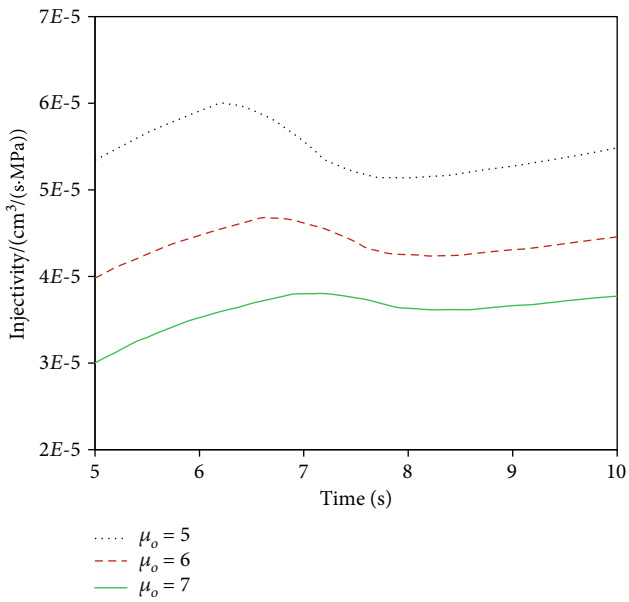

Figure 5: Injectivity change with time for different oil viscosity.

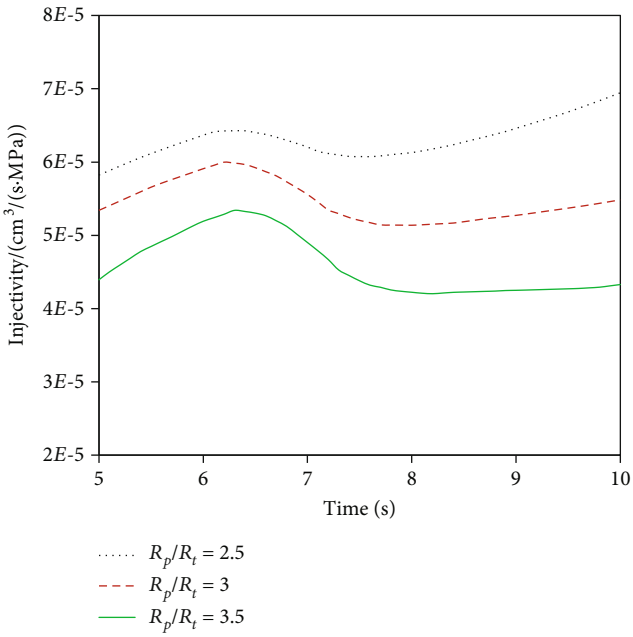

Figure 6: Injectivity change with time for different pore-throat ratio.

in the throat is large, after the water flooding front passes through throat, the rising rate of water injectivity will decrease with the increase of pore throat ratio.

4.2.3. CO_2 Slug Size. Because CO_2 is injected with constant pressure, the size of CO_2 slug cannot be changed by changing the CO_2 injection rate. However, CO_2 slugs with different sizes can be equivalently injected by setting different injection times. According to this treatment method, CO_2 injection time is set to be 4 s, 5 s, and 6 s, and then, different CO_2 slug size is obtained. After CO_2 injection, the changes of injectivity with time are shown in Figure 7.

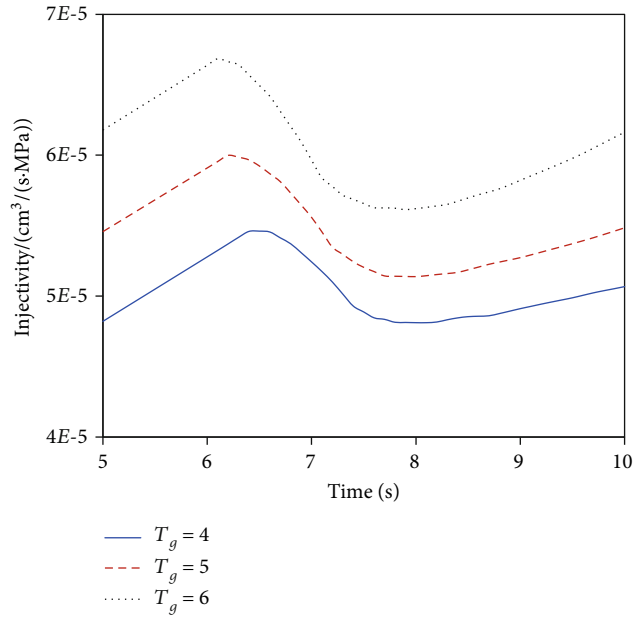

Figure 7: Injectivity change with time for different CO_2 slug size.

The larger the CO_2 injection time is, the longer the CO_2 slug is formed, and the smaller the total seepage resistance of the fluid in the capillary bundle is, so the injection capacity increases with the injection time. The throat is closer to the injection end, and the injection capacity increases linearly before the front of the water drive enters the throat. When the front edge of the water drive enters the throat, the injectivity decreases sharply. When the water drive front passes through the throat, the injectivity will increase slowly.

4.2.4. Equivalent Permeability. Since the pore throat ratio between the capillary and the throat is constant, the capillary radius distribution range in the capillary bundle is changed, and the equivalent permeability under different capillary bundles can be obtained by Equation (71), which is 10.6×10^{-3} μm^2, 18.5×10^{-3} μm^2, and 28.5×10^{-3} μm^2. The injectivity is calculated at different permeability, and the resulting injection capacity changes with time are shown in Figure 8.

As can be seen from Figure 8, the smaller the equivalent permeability (the smaller the range of the capillary bundle radius) is given, the smaller the injectivity will be. The reason is that for crude oil with the same viscosity, the smaller the equivalent permeability, the greater the resistance to be overcome by the fluid flow. Under the same injection pressure difference, the smaller the injection flow rate, the lower the injection capacity. This change law indicates that for low-permeability reservoirs, the injection capacity is lower due to the smaller pore throat, and the required injection pressure difference is greater at the same injection amount compared with the high-permeability reservoir. Under the same injection amount, the required water injection pressure difference is larger. If the fluid is injected with constant pressure, it is hard to inject water, which has an impact on the oil recovery for low-permeability reservoirs. Comparing Figure 5 to Figure 8, it can be found that the change of equivalent permeability has the greatest influence on the injection capacity,

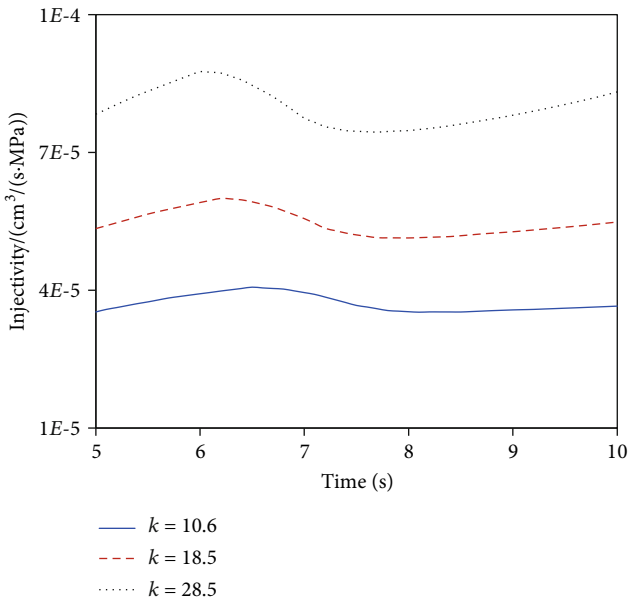

Figure 8: Injectivity change with time for different capillary tube radius.

which also indicates that in a practical pilot test for CO_2-alternating-water injection, the influence of permeability on injectivity should be fully considered.

5. Conclusions

(1) Considering the seepage, mass transfer, and CO_2 diffusion during CO_2 flooding, a mathematical model of convection-diffusion is established and solved. The relationship between the width of the mixed-phase zone and the injection time is obtained

(2) According to the difference of distribution forms for the unswept oil region, mixed-phase zone, CO_2 region, and water region in a capillary tube, six possible patterns are defined during CO_2 displacement, and three distribution patterns are described during water flooding. Through the introduction of the equivalent resistance model, the injectivity for each possible distribution pattern is evaluated during water-alternating-gas displacement

(3) Through parameter analysis, the injectivity decreases with the increase of crude oil viscosity and pore throat ratio. Oppositely, the injectivity increases with the equivalent permeability and CO_2 slug size. The equivalent permeability has the greatest influence on injection capacity compared with other factors; therefore, in practice, the influence of permeability on injectivity should be carefully considered

Data Availability

The data used to support the findings of this study are available from the first author upon request.

Conflicts of Interest

The authors declare that they have no conflicts of interest.

Acknowledgments

This study was supported by the National Science Foundation (51804328 and 51974348), the Fundamental Research Funds for the Central Universities (18CX02168A), and the European Union's Horizon 2020 Research and Innovation Program (846775).

References

[1] J. R. Christensen, E. H. Stenby, and A. Skauge, "Review of WAG field experience," *SPE Reservoir Evaluation & Engineering*, vol. 4, pp. 97–106, 2013.

[2] R. L. Henry, G. L. Feather, L. R. Smith, and D. D. Fussel, *Utilization of composition observation wells in a West Texas CO_2 pilot flood*, 1981.

[3] J. Zhao, J. Zheng, X. Hu, Z. Song, and P. Chen, "The WAG-surfactant flooding applied in the high-water-cut oil field: taking QK17-2 oilfield as an example," *Applied Science and Technology*, vol. 44, no. 4, pp. 75–77, 2017.

[4] M. Meng and Z. Qiu, "Experiment study of mechanical properties and microstructures of bituminous coals influenced by supercritical carbon dioxide," *Fuel*, vol. 219, pp. 223–238, 2018.

[5] M. Dong, J. Foraie, S. Huang, and I. Chatzis, "Analysis of immiscible water-alternating-gas (WAG) injection using micromodel tests," *Journal of Canadian Petroleum Technology*, vol. 44, no. 2, pp. 17–25, 2005.

[6] J. Wang and M. Dong, "Trapping of the non-wetting phase in an interacting triangular tube bundle model," *Chemical Engineering Science*, vol. 66, no. 3, pp. 250–259, 2011.

[7] J. Jovanović, W. Zhou, E. V. Rebrov, T. A. Nijhuis, V. Hessel, and J. C. Schouten, "Liquid–liquid slug flow: hydrodynamics and pressure drop," *Chemical Engineering Science*, vol. 66, no. 1, pp. 42–54, 2011.

[8] M. Piri, *Pore-Scale Modelling of Three-Phase Flow*, Imperial College London, London, 2003.

[9] Y. Yang, Z. Yen, J. Yao, Y. Li, and C. Wang, "Porescale simulation of microcosmic flow during water-alternating-gas(-WAG) in porous media," *Earth Science Journal of China University of Geosciences*, vol. 38, no. 4, pp. 853–858, 2013.

[10] J. O. Helland and S. M. Skjæveland, "Three-phase mixed-wet capillary pressure curves from a bundle of triangular tubes model," *Journal of Petroleum Science and Engineering*, vol. 52, no. 1-4, pp. 100–130, 2006.

[11] W. Jinan, Y. Guangjun, Z. Jun, and X. Fengting, "Experimental study on physical modelling of crude displacement with carbon dioxide drive for long core," *Special Oil & Gas Reservoirs*, vol. 2, 2001.

[12] M. Zhao and C. Liu, "The effect of CO_2 injection process on production response of Fang-48 Reservoir in Daqing Oilfield," *Xinjiang Petroleum Geology*, vol. 27, no. 4, pp. 449–451, 2006.

[13] M. Zhao, X. Ding, and J. Li, "Injection parameter's optimization of water-CO_2 displacement in low permeable oilfield," *Science Technology and Engineering*, vol. 27, p. 046, 2012.

[14] M. K. Zahoor, M. N. Derahman, and M. H. Yunan, "WAG process design–an updated review," *Brazilian Journal of Petroleum and Gas*, vol. 5, no. 2, pp. 109–121, 2011.

[15] J. Prieditis, C. R. Wolle, and P. K. Notz, "A laboratory and field injectivity study: CO_2 WAG in the San Andres formation of West Texas," in *SPE Annual Technical Conference and Exhibition*, Society of Petroleum Engineers, 1991.

[16] J. Kamath, F. M. Nakagawa, R. E. Boyer, and K. A. Edwards, "Laboratory investigation of injectivity losses during WAG in West Texas dolomrites," in *SPE Permian Basin Oil and Gas Recovery Conference*, Society of Petroleum Engineers, 1998.

[17] M. K. Roper Jr., C. T. Cheng, J. E. Varnon, G. A. Pope, and S. Kamy, "Interpretation of a CO_2 WAG injectivity test in the San Andres Formation using a compositional simulator," in *SPE/DOE Enhanced Oil Recovery Symposium*, Society of Petroleum Engineers, 1992.

[18] M. K. Roper Jr., G. A. Pope, and K. Sepehrnoori, "Analysis of tertiary injectivity of carbon dioxide," in *Permian Basin Oil and Gas Recovery Conference*, Society of Petroleum Engineers, 1992.

[19] D. Yang, C. Song, J. Zhang, G. Zhang, Y. Ji, and J. Gao, "Performance evaluation of injectivity for water-alternating-CO_2 processes in tight oil formations," *Fuel*, vol. 139, pp. 292–300, 2015.

[20] J. Li, T. Jang, W. Gao, and B. Liu, "Analysis and optimization of injection capacity of gas-water alternate flooding reservoirs," *Journal of Southwest Petroleum University*, vol. 30, no. 6, pp. 121–125, 2008.

[21] X. Zhou, X. Liao, X. Zhao, J. Gao, and B. Luo, "Laboratory investigation of miscible CO_2 WAG process in permeability reservoir," *Journal of Shaanxi University of Science & Technology (Science Edition)*, vol. 34, no. 6, pp. 120–124, 2016.

[22] X. Yan, C. Wang, and G. Zhang, "Optimization of injection parameters for CO_2 gas water alternative drive," *China's Manganese Industry*, vol. 35, no. 5, pp. 97–99, 2017.

[23] H. Hu, M. Ma, and G. Li, "Establishment of single phase seepage model of low-permeability capillary bundle," *Journal of Chongqing University of Science and Technology (Natural Sciences Edition)*, vol. 13, no. 3, pp. 93–95, 2011.

[24] Y. Xu, *Experimental Study on CO_2 Gas-Water Displacement in Low Permeability Reservoir*, Southwest Petroleum University, Chengdu, China, 2016.

[25] M. Du and G. Liu, "Analysis on factors of enhancing oil recovery by CO_2 and water alternating flooding in low permeability reservoirs," *Liaoning Chemical Industry*, vol. 46, no. 4, pp. 354–356, 2017.

[26] P. Guo, L. Huo, B. Jiang, and Y. Lei, "Parameter optimization of water alternating gas of Fang 48 CO_2 flooding pilot area," *Journal of China University of Petroleum (Edition of Natural Science)*, vol. 36, no. 6, pp. 89–93, 2012.

[27] H. Liao, "Numerical simulation of oil displacement with carbon dioxide in DB34 well block, Yaoyingtai Oilfield," *Journal of Xi'an Shiyou University, Natural Science Edition*, vol. 25, no. 5, pp. 50–53, 2010.

[28] M. Meng, Z. Zamanipour, S. Miska, M. Yu, and E. M. Ozbayoglu, "Dynamic stress distribution around the wellbore influenced by surge/swab pressure," *Journal of Petroleum Science and Engineering*, vol. 172, pp. 1077–1091, 2019.

[29] B. Dong, M. Meng, Z. Qiu, Z. Lu, Z. Ye, and H. Zhong, "Formation damage prevention using microemulsion in tight sandstone gas reservoir," *Journal of Petroleum Science and Engineering*, vol. 173, pp. 101–111, 2019.

[30] J. O. S. Pizarro and L. W. Lake, "Understanding injectivity in heterogeneous reservoirs," in *SPE/DOE Improved Oil Recovery Symposium*, Society of Petroleum Engineers, 1998.

[31] H. Hoteit, "Modeling diffusion and gas–oil mass transfer in fractured reservoirs," *Journal of Petroleum Science & Engineering*, vol. 105, pp. 1–17, 2013.

[32] Y. Su, *Reservoir displacement mechanism*, Petroleum Industry Press, Beijing, 2009.

[33] A. Leahy-Dios and A. Firoozabadi, "Unified model for nonideal multicomponent molecular diffusion coefficients," *AICHE Journal*, vol. 53, no. 11, pp. 2932–2939, 2010.

[34] C. Zhang, W. Sun, J. Yang et al., "Pore and pore-throat size distributions of low permeability sandstone reservoir and their differential origin," *Acta Geologica Sinica*, vol. 86, no. 2, pp. 335–348, 2012.

[35] M. Hu, "Study and application of microporous structure characteristics of low permeability reservoir," *24/5000 Langfang: Graduate School of Chinese Academy of Sciences (Institute of Seepage Fluid Mechanics)*, 2006.